Temperature Behaviour and Uniformity of SCT Barrels during Assembly and Reception Testing

Georg Viehhauser[1], Bettina Mikulec[2], Anna Sfyrla[2], Andree Robichaud-Veronneau[2]

[1]Oxford University, UK

[2]DPNC, University of Geneva, Switzerland

ATL-INDET-PUB-2006-009

08 November 2006

1. Introduction

This note presents temperature studies of the barrel SemiConductor Tracker (SCT) modules during the barrel assembly at Oxford University and the barrel reception at CERN. At Oxford, warm and/or cold tests have been performed on each of the four SCT barrels comprising a total of 2112 silicon strip modules [1]. After macro-assembly, the barrels were shipped to CERN where reception tests took place before the inner detector integration phase.

We present the temperature uniformity of the different barrels under changing operating conditions. Estimates of the errors contributing to the temperature measurements will be discussed. We introduce corrections for several systematic effects. We finally identify modules operating at higher temperatures and discuss possible reasons for their deteriorated thermal performance.

2. Cooling geometry

The macro-assembly of the ATLAS SCT at Oxford University comprised the mounting of individual detector modules [1] onto cylindrical carbon fibre support structures (barrels). Four concentric barrels form the barrel SCT (labelled B3 to B6).

In this note we identify modules azimuthally by the number of their corresponding Low-Mass Tape (LMT). LMTs are numbered 1-32, 1-40, 1-48 or 1-56, for the barrels B3 to B6, respectively[1]. Longitudinally modules are identified through their position along z (1 to 12 from –z to +z).

One cooling loop cools modules on four rows (Figure 1). Each loop consists of two u-shaped staves. The two staves are connected on the output side in a manifold. There is one input for each stave and one common output per loop as part of the manifold, such that all connections are on one end of the loop. The first module on a stave neighbours the last module on the same stave in the next row. The section of pipe servicing a complete row of modules will be referred to as a “pipe”. Each Cu/Ni pipe has a break in the centre, where a Cu/Ni sleeve has been soldered over the break. The outer diameter of the cooling pipe is 4.2 mm and the wall 70 µm thick.

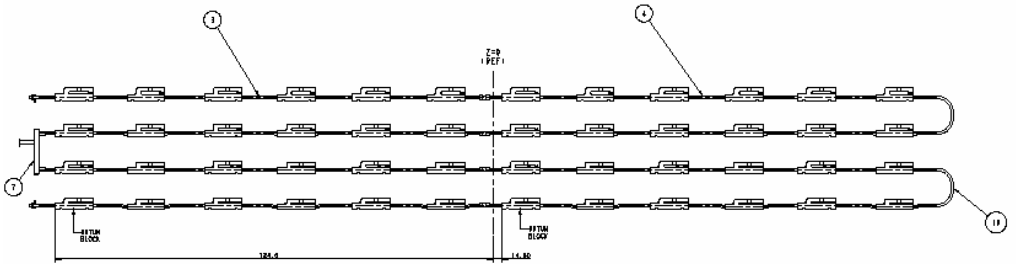

Figure 1: Cooling loop. In this drawing the two inputs and the output are to the left.

[1] These correspond to rows on the barrel. Note that there are two LMTs in each row, servicing the modules in –z and +z, respectively.

On each barrel the first loop is connected to LMTs 2-5. The inputs and the output are on the positive z-end for B3 and B4 and on the negative z-end for B5 and B6. Consecutive cooling loops have their connections on alternating ends of the barrel.

Each stave has two thermistors glued to a clamp fixed around the pipe close to the manifold. The main task of these sensors is to trigger an interlock failure if their temperature increases above threshold. Data from these sensors are recorded by the Detector Control System (DCS), but are not recorded by the DAQ.

Each input is connected to a capillary, along which most of the pressure drop between feed and evaporation pressure takes place. The capillaries used at Oxford were 2.8 m long and had an inner diameter of 1.3 mm.

3. Results from the SCT macro-assembly at Oxford

3.1. Cooling operating parameters

Estimated operating parameters of the cooling system at Oxford are listed in Table 1. During the assembly at Oxford the barrels were tested in two different configurations:

(a) Shortly after the completion of mounting of modules for a given loop the modules were tested with perfluorobutane (C_4F_{10}, R610) as a coolant. Typically the evaporation temperatures in this mode were between 10° and 15°C. This configuration is referred to as “warm”. The largest group of modules tested in this way corresponded to one cooling loop, although tests of smaller groups, depending on the progress of assembly, were quite common. The intervals between these tests could be up to weeks. In particular, tests of smaller groups were frequent during the assembly of the first barrel, B3.

(b) After the completion of the module mounting for a given barrel a test of the complete barrel was performed. During these tests the coolant was octofluoropropane (C_3F_8, R218) evaporating at a temperature between -8° and -3°C. This operating mode is referred to as “cold”. No cold test of B5 was performed at Oxford.

The evaporation temperature was controlled by backpressure regulators. Typically the limiting factor in temperature was the dew point in the large cold room at Oxford and the backpressure regulators were adjusted so that the temperature sensors on the cooling pipe exhausts measured a temperature well above the dew point.

During operation we observed significant pressure drops between the end of the cooling loop and the backpressure regulators. This was probably dominated by the flexible tubing connecting the barrels to the cooling pipe manifolds in the floor of the assembly area. These were pipes with 6 mm inner diameter (ID) for B3, which were then changed to 10 mm ID pipes for the later barrels. The presence of liquid was visible up to the heaters, which were between 1.2 m and 2 m higher than the lowest pipes in the return pipework, and up to 0.5 m higher than the top of the barrel.

The instrumentation of the cooling system used during the assembly with sensors was crude, as the purpose of this system was cooling of the modules for checks of their electrical performance after mounting, and not a systematic study of an evaporative cooling system. We therefore have only poor estimates of the mass flow at any given time in the system.

Vapour quality estimates are noted in Table 1. Note that for electrical operation of smaller subsets of modules (e.g. one row per stave, one half of the barrel) the output vapour quality was lower than listed there.

Table 1: Cooling system operating parameters (estimated) during assembly at Oxford.

	Warm	Cold
Coolant	C_4F_{10}	C_3F_8
Pre-cooling	Not as part of the cooling system. See vapour quality	
Backpressure	~1.5 bar_a (at backpressure regulator)	~3 bar_a (at backpressure regulator)
Power per loop	Total power per stave dissipated in the heater was about 250-300 W (module power off).	Total power per stave dissipated in the heater was about 400 W (module power off).
Mass flow per loop	Around 3-5 g/s.	No reliable measurement
Vapour quality	Due to the special cycle (condensation at lower temperature than evaporation) the input vapour quality was likely to be close to 0. The output vapour quality was close to 1 for fully powered loops as operation was close to dry-out. The data presented here was taken with one half of each loop powered at any time ($x_{out} \approx 0.5$)	Although no pre-cooling by design, coolant was supplied through cold room at ~ -5°C. How much enthalpy the liquid lost during the approach is difficult to estimate. Output vapour is estimated to be for most of the data around 0.9.
Ambient	~20-22°C	~ -5°C

3.2. Data for the Oxford runs

The temperature of the hybrids on the SCT modules is measured by two thermistors (Semitec 103KT1608-1P), one on the top and one on the bottom side of the module. The characteristic resistance of these thermistors is given by $R = R_{25}\exp\left(B\left(1/T - 1/T_{25}\right)\right)$ with $R_{25} = 10k\Omega \pm 1\%$ and $B = 3435K \pm 1\%$, where T_{25} and R_{25} are the properties at 25°C and temperatures are given in K.

The data from the thermistors are read out through the low voltage (LV) supply cards, from where they are transferred via CANbus to the PVSS-based DCS software projects. This program publishes the data via the Information Server (IS) that is part of the ATLAS read-out software. The information is updated approximately every 2 minutes.

During the assembly tests the DAQ software collected at the start of a run the latest information from the DCS through the Information Service (IS) and stored it before the actual data-taking began. These data were used for the analysis presented here. We do not analyze the data stored by the DCS itself.

The data for each barrel and in each configuration have been collected into single datasets. These datasets for the Oxford measurements can be found at http://www-pnp.physics.ox.ac.uk/~daquser/cgi-bin/showModuleMapData.cgi.

For each dataset data for a small number of modules was missing. These were typically modules that developed a fault and were replaced at a later stage of the assembly. The only dataset with a significant number of modules not recorded is the warm B3 data set, where the data from 8 half-rows are missing for unknown reasons.

3.3. Power and temperature gradients

In each module analogue and digital electrical power is transformed into heat. During the tests the supply voltages were V_{cc} = 3.5 V with $I_{cc} \approx 1$ A and V_{dd} = 4 V with $I_{dd} \approx 0.5$ A. Power consumption varied significantly during a run, depending on the activity of the module.

Total power distributions have been calculated from the monitored voltages and currents for the B6 cold test (Figure 2 and Figure 3). The average power per

module recorded for this data was 5635 mW, and the distribution has a standard deviation of 120 mW (2.1%).

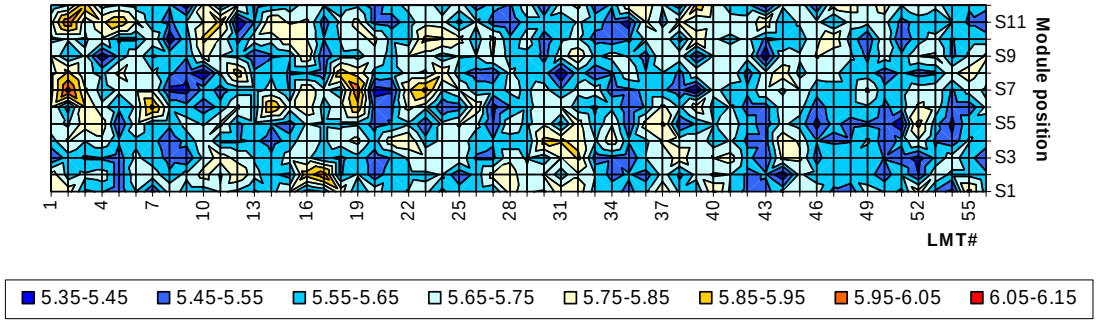

Figure 2: Map of electrical power (in W) supplied during B6 cold test.

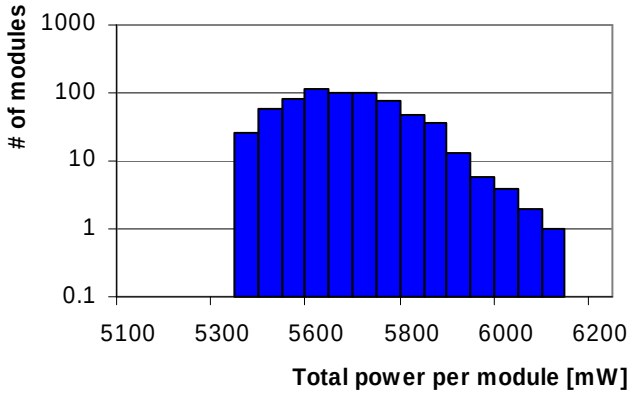

Figure 3: Module power distribution during B6 cold test.

Assuming that the coolant temperature is relatively accurately measured by the DCS thermistors, the temperature difference between the module hybrid thermistors and the coolant is about 18°C. A comparison with the observed average power of 5635 mW yields the thermal conductance of the heat diffusion thermal path through the module, grease joint, cooling block, cooling pipe wall and into the coolant of about 0.3 W/°C. The power fluctuations discussed above translate therefore into temperature variations due to power fluctuations of $\sigma_{power} \approx 0.4$°C.

3.4. Thermistors

To understand the systematics of the hybrid thermistors we studied the temperature difference $\Delta T = T_0 - T_1$, where T_0 and T_1 are the temperatures of the top and the bottom side of the hybrid, respectively. The results for the different data sets are given in Table 2. The temperature gradients are negative, implying that on average modules are hotter on the side facing the carbon fibre barrel (bottom) than on the outside (top).

Table 2: Temperature difference $\Delta T = T_0 - T_1$ between the upper and lower side of the module hybrids. The first column gives the average for each dataset and the second the standard deviation of this distribution. The last column lists the resulting estimate on the error of a single thermistor temperature measurement ($\sigma_{Therm} = \sqrt{2}\sigma_{\Delta T}$). Rows labelled "All" show distributions for all modules in the particular sample (not average of distributions per barrel).

	$\overline{\Delta T}$ [°C]	$\sigma_{\Delta T}$ [°C]	σ_{Therm} [°C]
B3 warm	-0.32	0.64	0.91
B3 cold	-0.37	0.60	0.85
B4 warm	-0.20	0.41	0.58
B4 cold	-0.28	0.38	0.54
B5 warm	-0.24	0.54	0.77
B6 warm	-0.40	0.85	1.20
B6 cold	-0.45	0.82	1.16
All warm	-0.30	0.66	0.93
All cold	-0.38	0.66	0.93
All	-0.33	0.66	0.93

There is a correlation between the cold and the warm data (Figure 4). A similar correlation, albeit slightly weaker, can be found using data from the module reception tests (Figure 5), during which the modules were in their transport boxes, cooled by a monophase cooling system at 14°C. In this case the heat was removed through a similar cooling block to that of the final geometry, but the cold mass of the module box enclosed the module symmetrically on both sides.

It therefore seems that the temperature difference is a property of the module. A possible explanation could be the way that the hybrid has been glued onto the module, where first the upper wing of the hybrid was glued, then the middle bend made and finally the lower wing glued to the baseboards. It is conceivable that it was difficult to maintain the specifications on the glue joint next to the bend and that would lead to increased thermal impedance at this location [2]. The temperature difference between the two sensors was measured at the module construction sites and only modules with $\Delta T < 2$°C were accepted for installation on B3, B4 and B5. For B6 this criterion was relaxed to 4°C.

An alternative explanation for the temperature gradient would be a different convective heat transfer for the two sides in the assembly, as the surface of the barrel was completely exposed. To investigate this possibility we studied the temperature difference as function of azimuthal angle for the cold datasets (see Figure 6). During these tests the barrels were roughly aligned as in ATLAS, namely so that LMT 1 is the first LMT above the horizontal plane. We would expect a different convective environment depending on the azimuthal angle. However, there is little indication of such an effect.

Also, warm data were in general taken in very different rotational orientation of the barrel. Nevertheless, there is a strong correlation between warm and cold data. This leads us to exclude the hypothesis that convection caused the temperature difference.

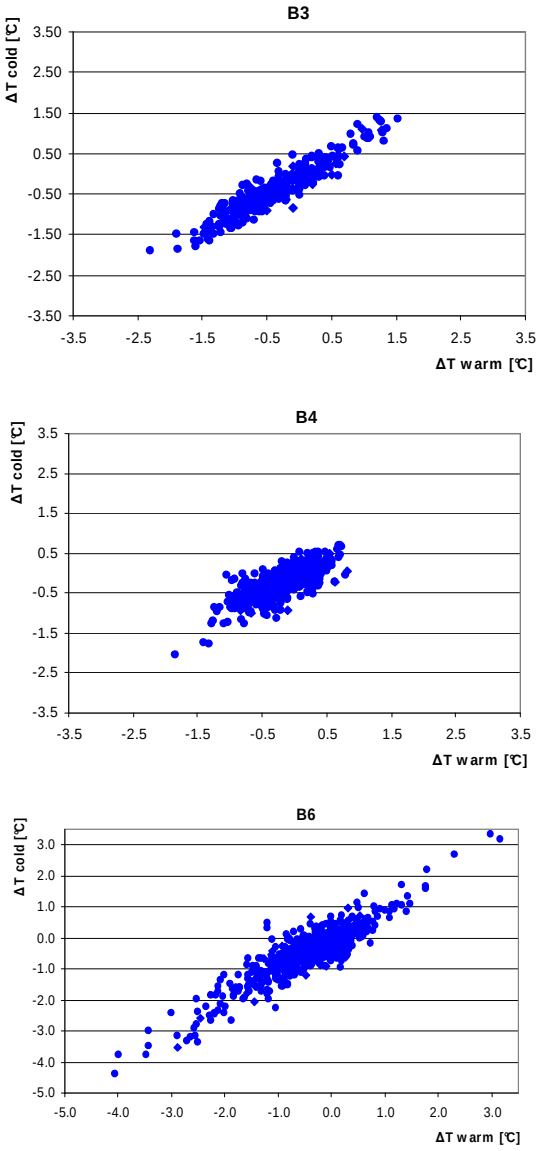

Figure 4: Temperature difference between module hybrid thermistors for warm and cold data.

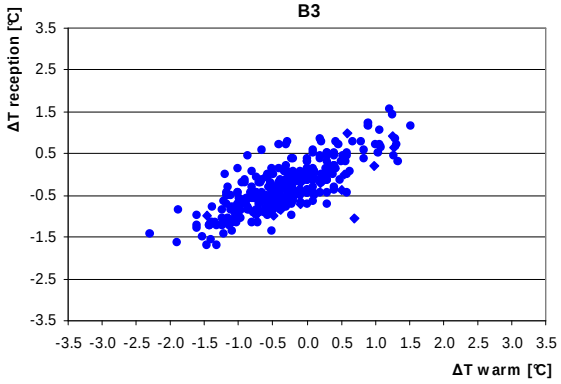

Figure 5: Temperature difference between module hybrid thermistors for reception and warm data for B3.

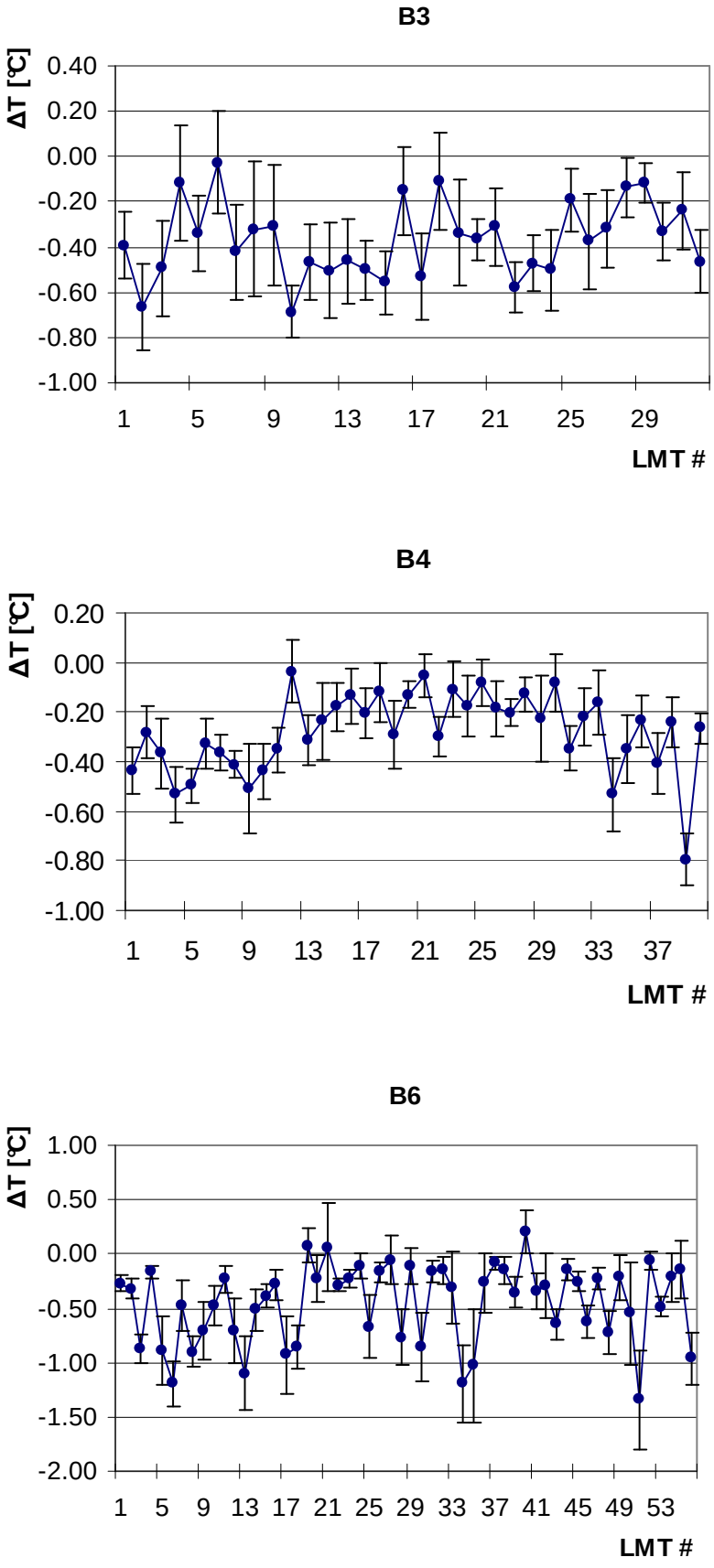

Figure 6: Temperature difference between hybrid thermistors averaged per LMT (note different scales).

There are three different components to the measurement error of the thermistors: a) a random error for the particular measurement of each thermistor (noise, digitization effects, etc.). b) a systematic bias on each thermistor, which comes from miscalibration or a difference in the thermal or electrical path, present in every measurement. In the data this will show up as a correlation between temperature differences measured in different runs (for example in the datasets for warm and cold data studied in this analysis). c) a systematic bias of the lower thermistors vs higher thermistors by 0.33°C present in all data.

We have attempted to disentangle the various contributions in Table 3 using the correlations between cold and warm data. For this we factored out correlated and uncorrelated temperature differences between the two datasets for B3, B4 and B6, warm and cold.

Table 3: Various contributions to the error of the module hybrid thermistor measurement per thermistor (assuming that all errors are the same for cold and warm data).

	σ_{Therm} (uncorrelated)	σ_{Therm} (correlated)	$\Delta T_{top-bottom}$
B3	0.15	0.86	-0.34
B4	0.19	0.49	-0.24
B6	0.32	1.09	-0.42

The origin for the differences in the three error contributions for the different barrels is not understood; partly they might be explained by the small number of datasets (two) we compared.

In the following we used the average of the upper and the lower temperature as the temperature of each module hybrid. The error on this combined measurement will be given as the combined error from the two thermistor temperature measurements averaged over all datasets (combined error $\sigma_T = \sqrt{2}\sigma_{Therm} = 0.66$°C). This error is compatible with the specifications of the thermistors.

3.5. Systematics of the absolute temperature measurements

Two systematic effects have been identified which distort the absolute measurement of the module hybrid temperature: The first are loop-to-loop fluctuations originating in the different evaporation pressure of each cooling loop. These fluctuations are caused by the inaccuracy of the backpressure regulators and by variations in the impedance in the return lines. In addition for the warm data the individual tests were done over the course of weeks, sometimes with significant changes in the cooling system parameters. The second effect is the temperature gradient inside a cooling loop dominated by the pressure gradient caused by the impedance of the cooling pipe. This second effect can be seen when the temperatures of all the modules corresponding to one position along a stave are averaged over a barrel and the temperature gradient along the stave is plotted (Figure 7). The observed gradients from a linear fit to the data are listed in Table 4.

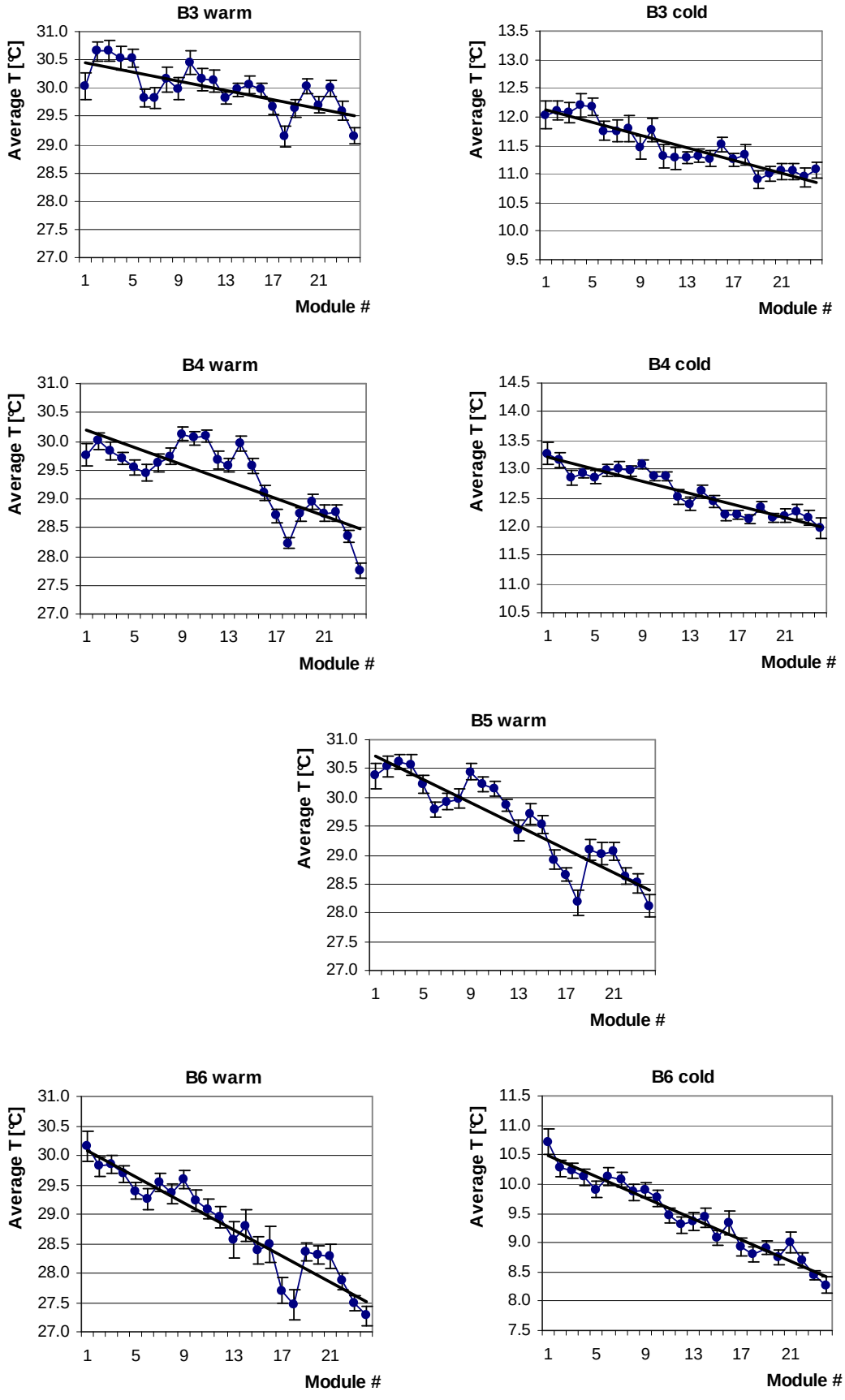

Figure 7: Average module hybrid temperature along a stave. Module 1 is right after the input, module 24 just before the output manifold. All plots have the same vertical span (4°C).

Table 4: Fitted average difference between hybrid temperature of the first and the last module in a stave.

	ΔT [°C]	
	warm	cold
B3	0.94 ± 0.20	1.25 ± 0.11
B4	1.71 ± 0.28	1.20 ± 0.10
B5	2.32 ± 0.23	-
B6	2.56 ± 0.20	2.06 ± 0.10

For comparison we have calculated the temperature drop along the pipe (frictional and momentum pressure drop) for the operating conditions described above, as well as the temperature gradient due to the heat transfer from the cooling pipe wall into the coolant[2]. Figure 8 shows the results of these calculations for a mass flow of 8.5 g/s of C_3F_8 in one complete cooling loop (p_{in} = 6 bar_a, T_{in} = 0°C, p_{evap} = 3.2 bar_a). The temperature difference between the first and the last module under these conditions is 2.1°C. The output coolant temperature is -7.7°C. It is difficult to estimate the pressure drops in the input and output pipes, as there was no pressure measurement at the detector. The same is true for the temperature of the incoming coolant. While the coolant left the condenser at the cold water temperature (~15°C), the amount of heat lost during the approach through the cold room cooled to about -5°C is difficult to estimate.

The magnitude of the temperature gradient depends strongly on the mass flow (the dependence is about 0.5°C/gs^{-1}), which unfortunately is badly known. The increase of temperature gradients for the different barrels could be explained by flow rate increases introduced during the assembly to make the cooling more stable.

Figure 8: Calculated temperature drop along a stave due to frictional and momentum pressure drop in the coolant (blue line) and of the cooling pipe wall (red line, includes coolant – wall heat transfer) for cold testing condition (C_3F_8, p_{in} = 6 bar_a, T_{in} = 0°C, p_{evap} = 3.2 bar_a). The comb structure of the cooling pipe temperature is caused by the non-uniform heat load due to the size of the cooling blocks.

[2] For the calculation of the pressure drop in two-phase flow we used the Friedel correlation, and to calculate the heat transfer to the tube wall the Chen correlation. For reference see [3].

A feature seen in the warm data are dips in the temperature distribution after the 6th and the 18th module along the stave. These can be explained by the fact that for the warm runs data sets with only one half of the barrel powered at any time were combined. In the case where the half of the barrel corresponding to modules 7-18 in a loop was powered, there was no power dissipated in the first stretch of the loop and the momentum pressure drop smaller, corresponding to an apparent higher temperature than module 6, when combined with the powered data for modules 1 to 6.

As a comparison we show the combined calculated temperatures for similar load configurations for a mass flow of 4.2 g/s of C_4F_{10} (p_{in} = 2.8 bar_a, T_{in} = 21°C, p_{evap} = 1.9 bar_a) in Figure 9. The overall temperature drop in this configuration is 1.8 °C and the output coolant temperature 14.7 °C. Note the apparent temperature changes between modules 6 and 7 and 18 and 19. Our model does not include heat loss due to free convection or radiation, which is likely to decrease the temperatures of modules at the ends of a powered group (1, 6, 7, 12, 13, 18, 19 and 24 in this configuration).

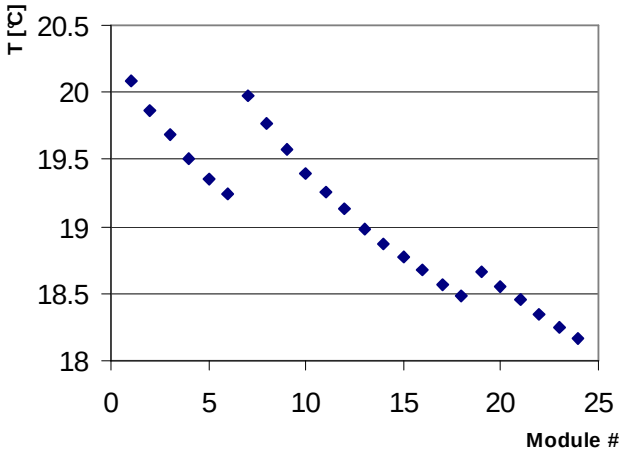

Figure 9: Calculated temperature profile of cooling pipe wall temperature for combined data of half-barrel load configuration.

In the following we correct for loop-to-loop variations (one constant per data set per cooling loop) and a linear drop of the temperature in the cooling loop (one slope per data set for all the loops), but not for the additional dips in the warm data.

3.6. Temperature variations of the SCT barrels during macro-assembly

The distributions of the module hybrid temperatures for the different data sets after the corrections described above can be seen in Figure 10. Table 5 lists the average temperatures and the standard deviations of the temperature distributions. Figure 11 shows correlations between cold and warm data, where available. Figure 12 displays maps of the temperatures in the different datasets.

Table 5: Average hybrid temperature variations and standard deviation of the module hybrid temperature variations after different corrections of systematic effects. All corrections include correction of loop-to-loop variations and of linear temperature variation within a stave.

	$\overline{T}$ [°C]	Raw data σ_T [°C]	Loop-to-loop corrected σ_T [°C]	All corrections σ_T [°C]
B3 warm	29.95	0.97	0.77	0.72
B3 cold	11.49	1.45	0.96	0.88
B4 warm	29.34	1.01	0.95	0.79
B4 cold	12.60	0.78	0.70	0.60
B5 warm	29.56	1.47	1.15	0.91
B6 warm	28.79	1.54	1.32	1.07
B6 cold	9.45	1.31	0.99	0.77

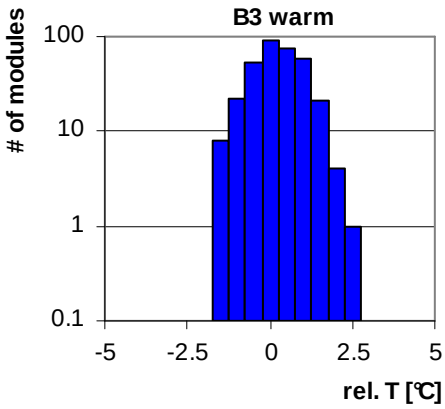
B3 warm
# of modules
100
10
1
0.1
-5
-2.5
0
2.5
5
rel. T [℃]

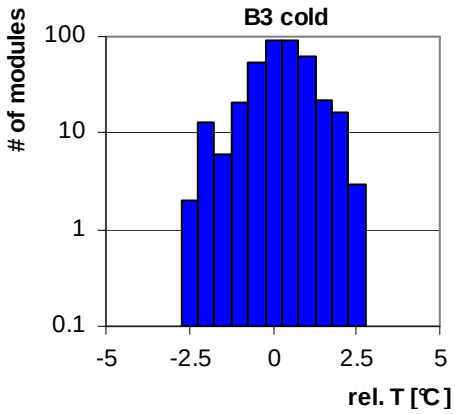
B3 cold
# of modules
100
10
1
0.1
-5
-2.5
0
2.5
5
rel. T [℃]

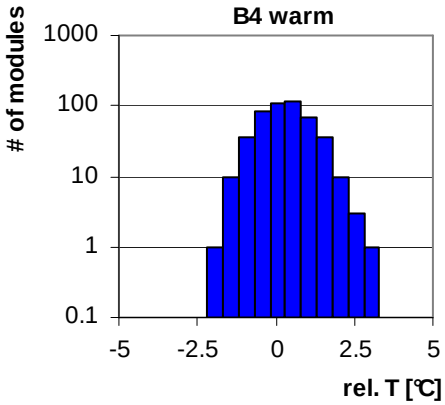
B4 warm
# of modules
1000
100
10
1
0.1
-5
-2.5
0
2.5
5
rel. T [℃]

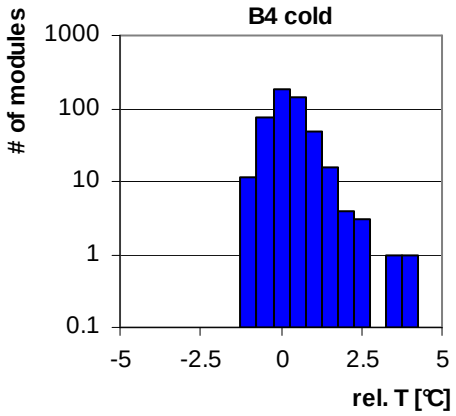
B4 cold
# of modules
1000
100
10
1
0.1
-5
-2.5
0
2.5
5
rel. T [℃]

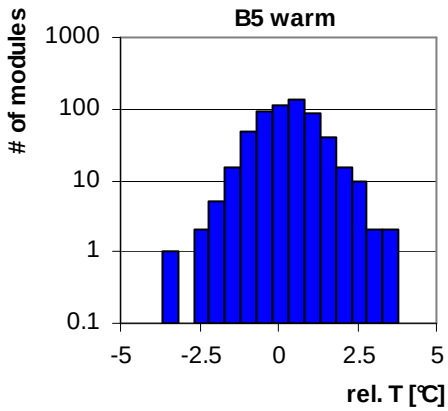
B5 warm
# of modules
1000
100
10
1
0.1
-5
-2.5
0
2.5
5
rel. T [℃]

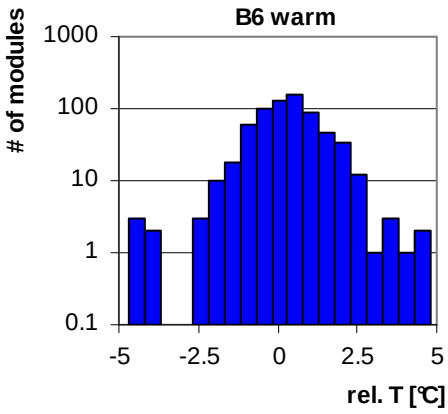
B6 warm
# of modules
1000
100
10
1
0.1
-5
-2.5
0
2.5
5
rel. T [℃]

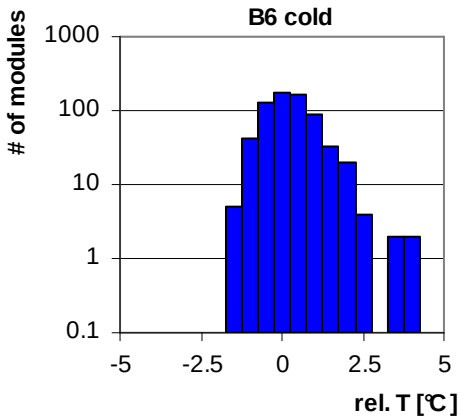
B6 cold
# of modules
1000
100
10
1
0.1
-5
-2.5
0
2.5
5
rel. T [℃]

Figure 10: Relative module hybrid temperature variations after correction of systematic effects. The histograms have no under- or overflows.

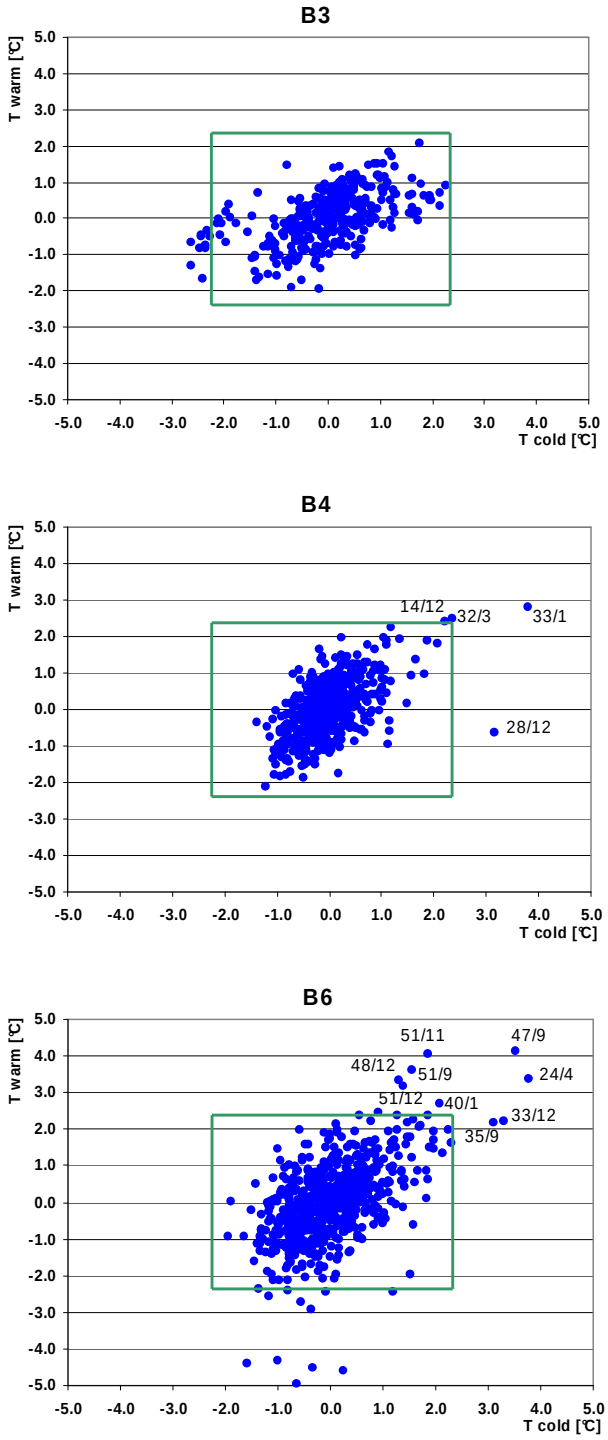

Figure 11: Correlation between cold and warm datasets for relative module hybrid temperature after corrections. The green box indicates the limits described in the text. Hot modules are identified by LMT number/position along z.

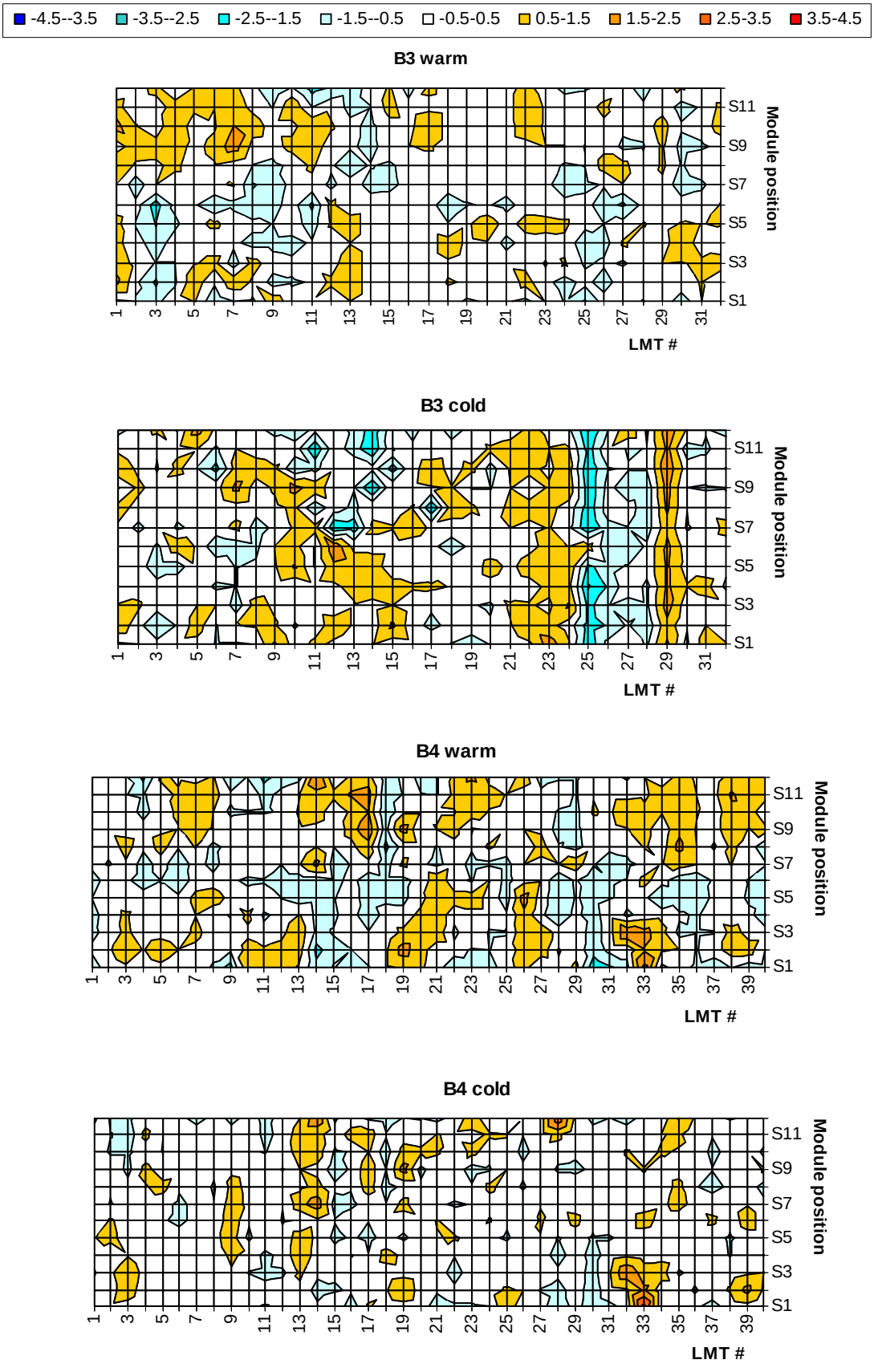
-4.5--3.5
-3.5--2.5
-2.5--1.5
-1.5--0.5
-0.5-0.5
0.5-1.5
1.5-2.5
2.5-3.5
3.5-4.5
B3 warm
B3 cold
B4 warm
B4 cold
Module position
LMT #
S1
S3
S5
S7
S9
S11

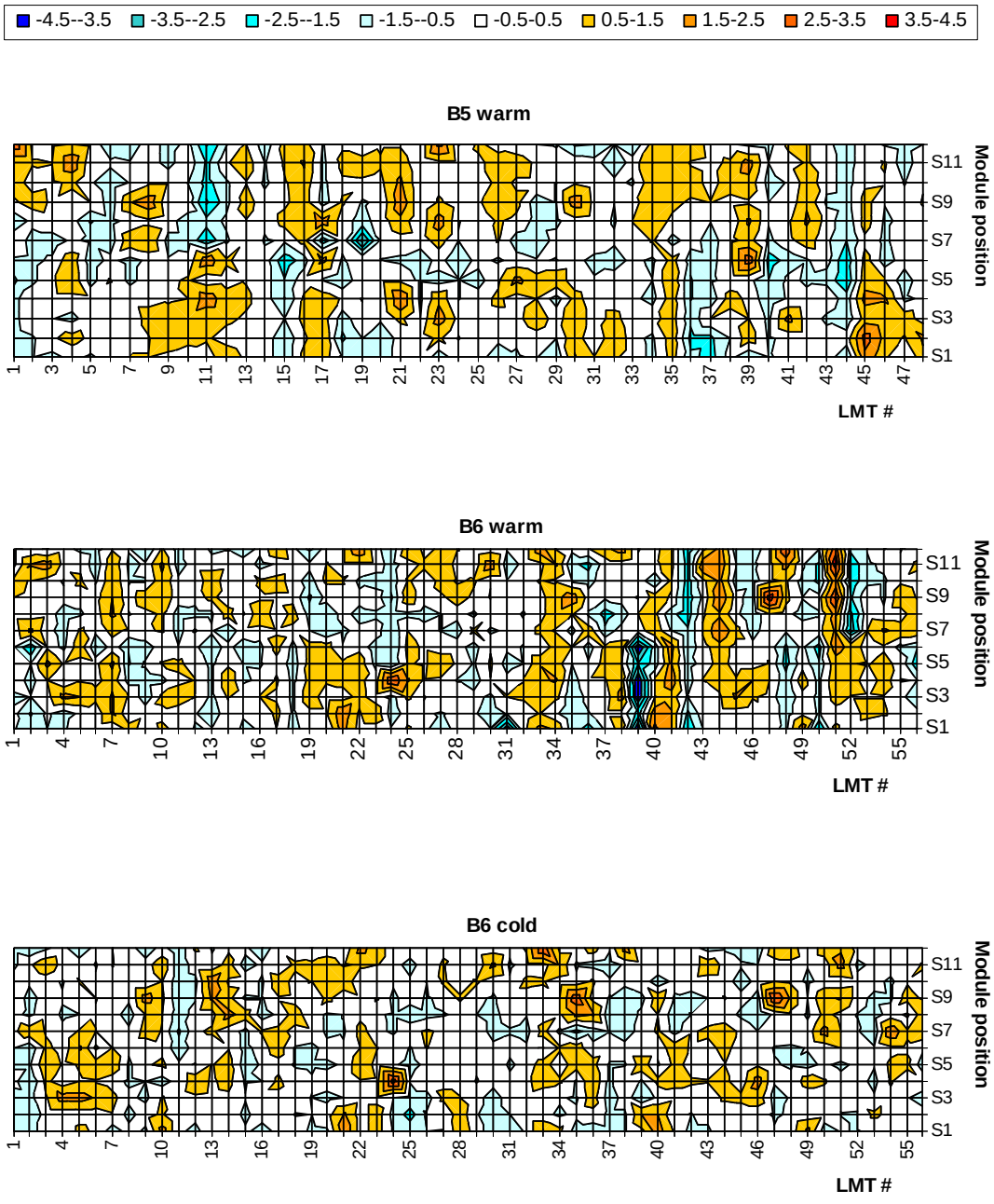

Figure 12: Relative temperature maps (in °C) for the different datasets after corrections.

3.7. Temperature and power correlations

We attempted to correlate the recorded power data with the thermistor measurements, but have failed here to find a correlation (Figure 13). The reason for this failure is not understood, but might lie in asynchronous recording of the different data. To study this point further would require going back to the DCS archive and use the time tag supplied with the data points there. Even then it is not clear whether the LV card reads the data taken at the same time.

We therefore cannot calibrate out the power fluctuations of individual modules and the temperature variations they incur and have to allow for an error of 0.4°C caused by the power fluctuations on a barrel.

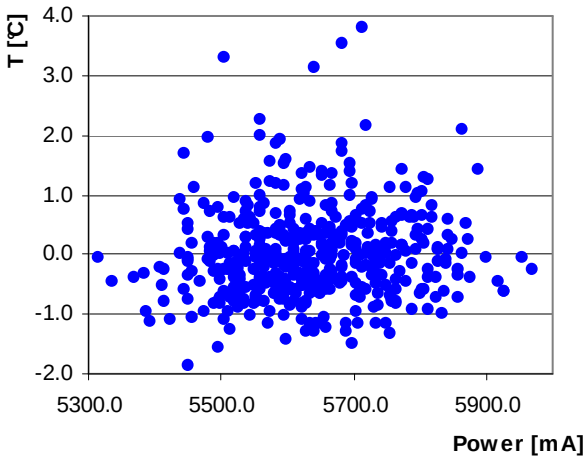

Figure 13: Module hybrid temperature vs. power supplied to the module for the B6 cold data.

3.8. Temperature outliers

The threshold that we have chosen to identify hot spots on the barrels is three times the combination of the thermistor measurement error and the temperature fluctuation due to power variations on the barrel:

$$T_{thresh} = 3\times\left(\sigma_{therm}/\sqrt{2} \oplus \sigma_{power}\right) = 2.28°\text{C},$$

with the error contributions as discussed in sections 3.4 and 3.3, respectively.

A list of the modules failing this criterion in at least one of the datasets is given in Table 6. We found 0, 4, 5 and 14 modules exceeding this threshold for the different barrels (0, 0.8%, 0.9% and 2.1%). In total these are 23 modules or 1.1%.

Critical points for hotter modules are next to the inlets or the outlets of the cooling loops. In total six modules next to an inlet, of which four are listed in Table 6, and three modules next to an outlet, all listed in Table 6 have been identified with higher temperatures. The likely cause for this is that due to the mechanical over-constraint the grease joint between cooling block and module suffers, as the orientation of the module is defined by the 3-point fixation on the brackets, whereas the cooling loop is constrained at the end flange. Misalignments between the two constraining systems increase the gap between the module baseboard and the cooling block, which has to be filled by thermally conductive grease. Further away from the end the compliance of the loop reduces the problem.

In addition to the modules listed in Table 6 B6 LMT 17 position 12 was found during assembly to be higher by 2°C than its neighbour during warm tests. Here, as in other cases, the mechanical connection of the pipe to the end-flange was loosened, the pipe was wiggled, and then the connection was retightened. The relative temperature data for this module after this procedure are 1.50°C (warm) and 0.32°C (cold). B6 LMT 54 position 12 had a 3°C higher temperature than its neighbour during warm testing. In this case we removed the module. The grease layer, although visually of nominal thickness, made contact over only a third of the surface. We applied a thicker grease layer and remounted the module. Our data for this module are now 0.54°C (warm) and 0.45°C (cold).

Another feature that shows a correlation with excess module temperatures is a large temperature difference between the two sensors. Five modules in Table 6 have a temperature difference larger than three times the standard deviation of the average

distribution for all the data sets. This could either be due to an unusually large miscalibration of one of the sensors which could bias the average temperature for the module, or could be due to the asymmetric thermal impedance in the heat path for the module. All these modules are on B6, where the module acceptance criteria were less stringent. To distinguish between these two hypotheses data taken without any power supplied to the module would be required. The large temperature differences are negative for all five 'hot' candidates, which points to a poor thermal connection on the glue joint of the lower bridge as outlined above.

For the remaining modules in Table 6 we have to conclude that they have some additional thermal impedance in the path of heat removal. A likely candidate for this would be a bad grease joint, although other sources cannot be ruled out with the existing data.

The nominal temperature gradient due to the thermal conductivity of the heat sink grease across the 0.1 mm thick grease layer for the power levels found above is 2.0 °C. An excess temperature of 4 °C therefore either means a three times thicker grease layer or a coverage of only one third of the contact area.

Table 6: 'Hot' modules during the assembly. Temperature T is the relative temperature above average for its position along the stave. ΔT is the temperature difference between the two (upper and lower side) thermistors on one module hybrid.

	Position LMT/pos	Module number	Warm T[°C]/ΔT[°C]	Cold T[°C]/ΔT[°C]	Comment
B3			none		
B4	14/12	20220330200691	2.41/-0.99	2.22/-0.86	
	28/12	20220170200368	-0.6/0.18	3.17/0.05	Output pipe
	32/3	20220170200256	2.48/-0.87	2.35/-0.49	
	33/1	20220170200231	2.79/0.82	3.80/0.05	Input pipe, loosened & retightened after cold test
B5	1/12	20220380200211	3.33/-0.71	-	Input pipe
	21/4	20220170200478	2.46/0.12	-	
	23/12	20220330200365	2.87/-0.11	-	Output pipe
	39/6	20220040200146	3.12/-0.11	-	
	45/2	20220380200046	2.98/-0.22	-	
B6	22/12	20220380200225	2.36/-0.11	1.86/-0.29	Input pipe, loosened & retightened after warm test
	24/4	20220170200913	3.38/0.32	3.78/0.04	
	33/12	20220040200151	2.20/-2.50	3.30/-2.38	Input pipe, large ΔT
	35/9	20220330200371	2.17/-3.48	3.12/-3.76	Large ΔT
	40/1	20220040200144	2.69/0.52	2.08/0.46	
	43/11	20220330200672	2.35/-1.32	1.28/-1.58	
	44/7	20220170200575	2.44/-0.40	0.91/-0.12	
	44/9	20220170200885	2.36/0.10	0.55/0.16	
	47/9	20220380200155	4.13/0.00	3.52/-0.17	
	48/12	20220040200315	3.34/-1.16	1.30/-1.75	Output pipe
	51/9	20220330200570	3.59/-2.65	1.55/-3.22	Large ΔT
	51/11	20220330200608	4.04/-2.5	1.85/-3.38	Large ΔT
	51/12	20220330200611	3.15/-4.05	1.39/-4.38	Large ΔT
	54/7	20220330200276	1.63/1.76	2.29/1.68	

3.9. Thermal imaging

During the operation of B4 pictures of the barrel were recorded with a thermal imaging camera (Jenoptik Varioscan 311). While it is difficult to derive exact quantitative results from such images, as this would require careful calibration of infrared reflectivities, these images confirm the high degree of uniformity in the thermal conductivity found in the numerical analysis (Figure 14).

Figure 14: Thermal Image of B4. Cold testing, complete barrel powered. The white crossing lines mark the position of the thermal profiles shown to the right and at the bottom. The bottom scale extends from 0.4°C to 8.8°C and the scale on the right from -4.4°C to 9.1°C.

4. Results from the SCT reception tests at CERN

Once all the modules were mounted on a barrel and accepted by the final macro-assembly tests at Oxford, the barrels were shipped to CERN where they underwent reception tests. These tests took place in the surface building 'SR1', where subsequently the four-barrel integration and the integration into the transition radiation tracker (TRT) were performed.

4.1. Cooling operating parameters

For the inner detector acceptance tests of the pixel and SCT subsystems of the ATLAS ID a cooling plant based on an evaporative C_3F_8 system was installed in SR1. The coolant passes in liquid phase from a tank through an internal heat exchanger and arrives at the two distribution racks (one per z-end) to which the barrel cooling loops are connected. After leaving the cooling loop, it passes through the second pipe of the internal heat exchanger, a heater, a backpressure regulator, the buffer tank and the compressor and ends in the condenser that closes the loop. External pre-cooling was optional, but was not used for the barrel reception tests. The evaporation temperature was controlled by the backpressure regulators and set such that there was a safe margin to the dew point. A DCS project monitored the liquid weight in the tank, input pressure, buffer pressure, the two backpressures (for the distribution racks at z+ and z-) and the two heater temperatures. Unfortunately, no measurement was available concerning the coolant temperature and pressure at the inlets of the cooling loops, the mass flow and the vapour quality.

4.2. Data for the barrel 3 reception tests at CERN

Due to schedule constraints, only barrels 3 and 5 were tested as a whole in SR1 with all 384 (B3) and 576 (B5) silicon modules cooled, powered and read out at once. During the B5 tests some parameters of the cooling plant were not tuned optimally resulting in a difference in hybrid temperatures of about 6°C between the first and the last module mounted on a cooling loop. Therefore we concentrate only

on the SR1 B3 data in this note. The data set used for the following analysis can be found at http://www-pnp.physics.ox.ac.uk/~daquser/cgi-bin/showModuleMapData.cgi?locn=CERN.

4.3. Results of the SR1 measurements

Due to different cooling system parameters used for the barrel reception tests in SR1 compared to Oxford, it is expected that some differences shall be observed in the overall thermal behaviour of the barrel. Nevertheless the comparison with the Oxford data should yield the intrinsic thermal behaviour of the modules as mounted.

The results presented below correspond to backpressure settings of 5.0 bar_a yielding average module temperatures of 25.88±0.77°C (from Fig. 15). The coolant temperature can be approximated by the temperature measured through the environmental DCS thermistors glued close to the cooling loop outlets. This was on average 13.5°C, yielding a temperature difference of about 12 degrees between coolant temperature and hybrid temperature. B3 was tested in a test enclosure flushed with dry air, and at room temperature of about 22°C. All modules on B3 were cooled and operated together.

Fig. 15 shows a 2-dimensional distribution of the average module temperature $T_{av}=(T_0+T_1)/2$ for the unfolded barrel during a typical B3 reception test. Three modules were excluded from the configuration (LMT4 z-2, LMT21 z+3, LMT25 z-1) due to temporary HV or LV problems; their temperature values were set to 26°C to avoid biasing the contour plot. One module (20220330200287 at LMT17 z+2) has an average temperature of 20.8°C, significantly lower than the others, without showing any additional problems. In this representation the first inlet is ‘at the top’ (z+) at LMT position 2, followed by the combined outlet (also at the top) of LMTs 3 and 4 and the second inlet of this cooling loop at LMT 5. The following cooling loop has its inlets and outlets ‘at the bottom’ (z-) of the figure and so on. There are a few areas with higher average temperature visible on this plot around LMTs 7-9 and 11-13; the ‘hottest’ regions are never in the first part of the inlet pipe, but rather in the part where the inlet pipe makes its turn towards the outlet (compare Fig. 1).

This is also visible when plotting the average module temperatures starting from modules mounted closest to inlets until the last module closest to an outlet, averaged over all staves (Fig. 16); modules around the centre of the plot show higher temperature values. For comparison, the same profile plot for one ‘hot’ stave (Fig. 17 left) and another typical stave (Fig. 17 right) has been included.

During all tests in SR1 we observed a slight temperature increase from inlet towards outlet, different than in the Oxford measurements. This behaviour can be attributed to different operational parameters of the cooling system.

Figure 15: 2-dimensional map of the average module temperatures for the unfolded B3. Hotter regions are visible around LMT 7-9 and 11-13.

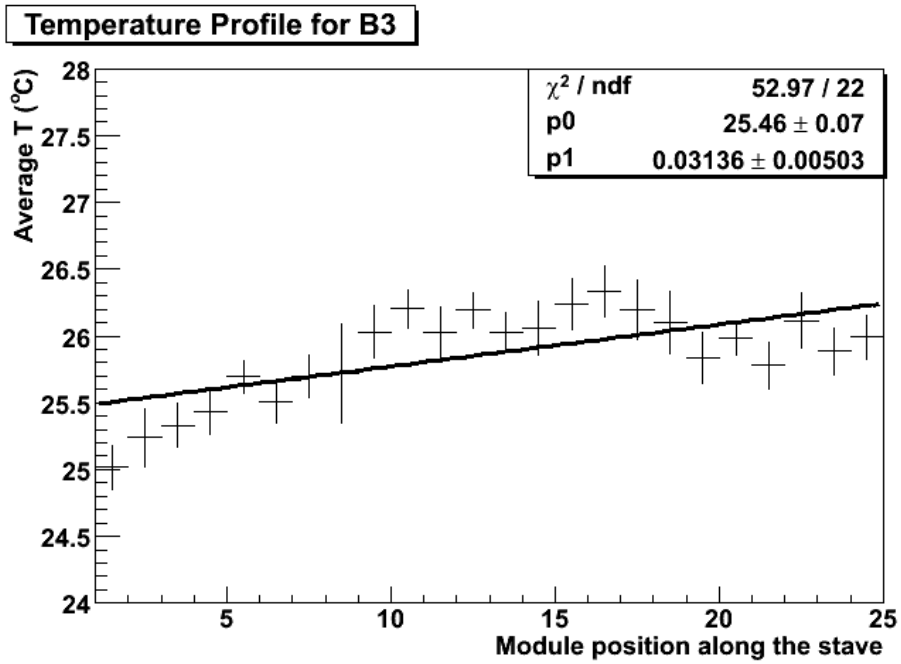

Figure 16: B3 temperature profile (T_{av}) along one stave (=one half cooling loop) from inlet to outlet averaged over all staves. A temperature increase towards the outlet is visible, different than in the Oxford results. In average, temperatures are highest around the bending region of the pipe.

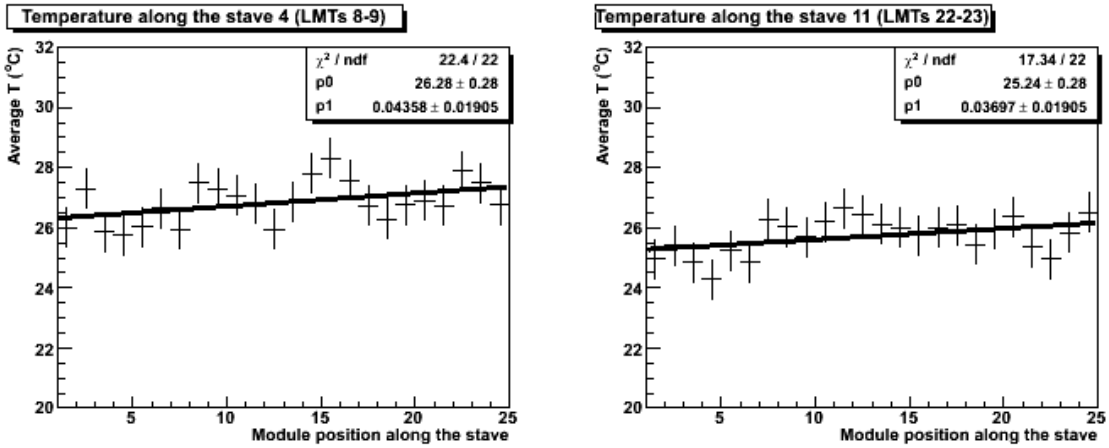

Figure 17: Average temperature profile along two selected staves; the left plot shows the stave of LMTs 8-9 including the hotter region, whereas the right plot shows a different typical stave (LMTs 22-23).

In an attempt to explain the hotter regions visible in Fig. 15, we here examined the distribution of the temperature differences T_0-T_1. During the reception tests B3 was positioned such that the hotter regions correspond to the area of the barrel located around 3 o'clock position with module orientations that might trap more heat underneath the module. However, no clear trend is visible (Figure 18), giving no indication for a possible temperature variation due to convection. A 2D plot of this temperature difference distribution is shown in Fig. 20 (left). Possible explanations for the large hotter regions could be slightly different back pressures due to impedance variations in the return lines.

Figure 18: Distribution of the temperature difference between top and bottom module thermistor.

In order to be able to compare the SR1 results with the Oxford results (Fig. 12), we applied a similar temperature correction to produce Fig. 19: first we corrected stave-by-stave for the slope between inlet and outlet, and subsequently the temperature offset was subtracted for each stave. This correction should allow removing temperature differences due to loop-to-loop fluctuations because of

different evaporation pressures as well as temperature gradients along a cooling stave because of impedance differences between cooling pipes. After this correction there are still some hotter areas visible, but it should be noted that the sigma of the temperature variation is still very small (0.65°C; see right Fig. 20).

Figure 19: 2-dimensional distribution of the relative hybrid temperatures after corrections for the B3 reception tests.

Figure 20: Left: Distribution of T_0-T_1 for B3 reception tests. Right: Distribution of the corrected average hybrid temperatures.

To investigate this further, we plotted the total power consumption for all the modules (see Fig. 21). The average power per module is 5531 mW with a standard deviation of 82 mW or 1.5% (Fig. 22). With a temperature difference between the module hybrid thermistors and the coolant of about 12°C this yields approximately 0.46 W/°C as thermal conductance of the heat diffusion path through the module, grease joint, cooling block, cooling pipe wall compared to 0.3 W/°C quoted earlier for the B6 cold data measurements at Oxford. As for the Oxford case, no clear correlation between hybrid temperature and module power could be observed.

Figure 21: Power distribution for B3 during the reception tests. The three blue regions correspond to the three excluded modules.

Figure 22: B3 power distribution; the average dissipated power is 5.53 W.

Taking into account the uniform power distribution shown in Fig. 21 and the fact that the same hotter regions seen in B3 (Fig. 19) exist in the Oxford "cold" data (where the barrel was rotated 90 degrees with respect to the SR1 tests corresponding to the 'ATLAS' situation), leads us to the conclusion that they seem to be due to differences in the thermal heat diffusion path (for example differences in thermal grease coverage, cooling block, fixation force, cooling pipe wall thickness).

5. Conclusions

Temperature data from the hybrid temperature sensors on the ATLAS SCT barrels taken during the macro-assembly at Oxford University and CERN have been studied. From these studies we conclude:

- On average barrel modules are slightly hotter (by about 0.35°C) on the side facing the carbon fibre cylinder (bottom) than on the other (top). The most likely explanation for this is a difference in the heat conductivity of the thermal path between heat sources and cooling pipe for the two sides. No evidence for a convection effect could be found.
- The measurement error for single thermistor measurements is about 1°C. This includes variations in the thermal conductivity of the heat path for a given hybrid as well as the thermistor miscalibration and digitization errors. The intrinsic thermistor measurement error seems to be well within specification.
- Systematic module temperature variations are caused by loop-to-loop variations – most probably due to back-pressure variations – and variations along the length of the cooling pipe due to the drop of evaporation pressure and changes of the heat conductivity from the pipe wall to the coolant due to the changing flow patterns along the cooling pipe. The temperature profile along the cooling pipe for the Oxford data drops as expected, whereas the data from CERN show an increase in temperature, which is not entirely understood, but might be explained by the high pressure operation.
- After removal of these systematic effects the module temperatures are very uniform. Only 1.1% of the modules have a temperature higher than 3σ above the average temperature. The likely cause for the elevated temperature readings are problems with the internal and/or external heat path. In most cases of external heat path problems, the module is next to an inlet or outlet of the cooling pipe, suggesting a problem with a mechanical over-constraint of the grease joint resulting in a wider cooling block – baseboard gap that could not be filled with the nominal amount of grease.
- No correlation between recorded module power levels and temperature could be found. This is likely to be caused by the badly controlled timing of the two measurements in the data used. A more thorough analysis of this would use the data archived by the DCS projects, which would include more accurate timing information of individual measurements. Such an analysis could also study the dynamic behaviour of the system.
- The thermal conductance of the thermal path between the heat sources (ASICs) and the coolant is about 0.3-0.5 W/°C.

Acknowledgements

The analysis presented in this note is only a tiny fraction of the work required to obtain our results. Obviously the biggest fraction has been done by the groups of excellent technicians and colleagues involved in the macro-assembly at Oxford and at CERN. The analysis relies on both the hardware and the DAQ and DCS systems designed and built by the ATLAS SCT collaboration. To name a few whose contributions made this possible: Abdel Abdesselam, Richard Apsimon, Alan Barr, Jose Bernabeu, Janet Carter, Bilge Demirkoz, Pamela Ferrari, Forest Martinez-McKinney, Andy Nichols, Heinz Pernegger, Eric Perrin, Peter Philips, Steve McMahon, Richard Nickerson, Dave Robinson and Heidi Sandaker.

References

[1] A. Abdesselam et al, "The Barrel Modules of the ATLAS SemiConductor Tracker", ATL-INDET-PUB-2006-005, accepted for publication by NIM A.

[2] Steve McMahon, private communication.

[3] John G.Collier and John R. Thome, "Convective Boiling and Condensation", 3rd ed., Clarendon Press, 1996.